





PHOTOLUMINESCENCE AND MAGNETIC ENHANCEMENT IN ZnSe QUANTUM DOTS VIA CONTROLLED COBALT DOPING

 Thi Diem Bui^{1*},  Quang-Liem Nguyen², Van Cuong Nguyen¹,  Trong Tang Nguyen¹,
 Huu Phuc Dang^{3*}

¹Faculty of Chemical Engineering, Industrial University of Ho Chi Minh City, Ho Chi Minh City, Vietnam

²Institute of Materials Science, Vietnam Academy of Science and Technology, Hanoi, Vietnam

³Faculty of Fundamental Science, Industrial University of Ho Chi Minh City, Ho Chi Minh City, Vietnam

*Corresponding Author E-mail: buihthidiem@iuh.edu.vn, danghuuphuc@iuh.edu.vn

Received September 1, 2025; revised October 1, 2025; accepted October 10, 2025

Co²⁺ ion-doped ZnSe semiconductor quantum dots (QDs) were synthesized in aqueous solution using starch as a surface stabilizer to ensure nanoparticle dispersion. Structural and compositional analyses using X-ray diffraction (XRD) and energy-dispersive X-ray spectroscopy (EDX) confirmed the successful incorporation of Co²⁺ ions into the ZnSe matrix. XRD and UV-visible absorption spectroscopy were used to determine the crystalline structure, lattice parameters, and particle sizes of Co-doped ZnSe QDs. The optical properties were analyzed using absorption and fluorescence spectroscopy, revealing a blue shift in the absorption peak with increasing Co concentration due to quantum confinement effects and changes in particle size. Photoluminescence (PL) analysis revealed dual emission peaks, corresponding to band-to-band recombination and Co-related defect states, with maximum luminescence efficiency observed at the 9% Co doping level. Beyond this concentration, the quenching effects attributed to the Co-Co interactions reduced the fluorescence intensity. Magnetic hysteresis measurements demonstrated that the Co-doped ZnSe QDs exhibited room-temperature ferromagnetism, with saturation magnetization increasing with co-doping concentrations of up to 12%. The ferromagnetic properties were ascribed to the exchange interactions between the Co²⁺ ions and the ZnSe matrix.

Keywords: ZnSe:Co; Starch surface stabilizer; Cobalt doped; Magnetic properties; Photoluminescence

PACS: 78.67.Hc, 78.55.-m, 75.50.Pp, 81.05.Dz

1. INTRODUCTION

Scientists have focused their research on semiconductor nanoparticles in recent decades because of their distinct features compared to bulk semiconductors [1, 2, 3, 4]. Scientists have focused their study on the fabrication process and physical and chemical properties of group II-VI semiconductor nanoparticles, which are direct bandgap semiconductors with high quantum efficiency and are suitable for lighting and energy conversion applications [2, 4]. ZnSe quantum dots (QDs) are among the most non-toxic and chemically stable II-VI semiconductors. ZnSe is an n-type, direct bandgap semiconductor with a band gap of ~2.75 eV in bulk material, a Bohr radius of ~3.8 nm, and a large exciton binding energy of ~21 meV [5]. ZnSe QDs have gained attention as promising nanotechnology materials in recent years. Owing to their significant optical and electrical characteristics [6–8], ZnSe QDs have a wide range of potential applications including light-emitting devices, solar cells, chemical sensors, biomedicine, photocatalysis, and energy storage [9–11].

ZnSe is an effective substrate for doping various contaminants. Transition metals are frequently doped with QDs to produce novel materials with electrical, magnetic, and optical characteristics [13, 14]. QDs doped with metal ions exhibit novel, intriguing, and exceptional features compared to those of undoped semiconductor nanoparticles. Metal-doped quantum dots (QDs) have a wide range of potential applications. This is because the emission of impurity ions frequently results in greater thermal and optical stabilities in many distinct substrates [14]. Quantum dots doped with additional metal ions such as Cr, Fe, Co, Ni, V, Cu, or Mn, contributed to reducing structural defects and improving existing device technologies such as spin-LEDs and magnetic memory. Furthermore, these materials frequently exhibit significantly longer fluorescence lifetimes than undoped semiconductors [15–17]. Despite these advantages, significant questions remain regarding the fabrication method and the material's physical properties. These issues stem from the fact that the fabrication method for doped semiconductor nanostructures is highly complex, making it challenging to obtain good optical and electromagnetic properties within the same material.

In this study, Co²⁺ ions were doped into ZnSe QDs to generate various electronic states in the bandgap, thereby enhancing and broadening the emission band. Furthermore, Co²⁺ ions are highly magnetic substances that improve the magnetic characteristics of materials. The impact of Co²⁺ ions on the structural, optical, and magnetic characteristics of ZnSe QDs was explored.

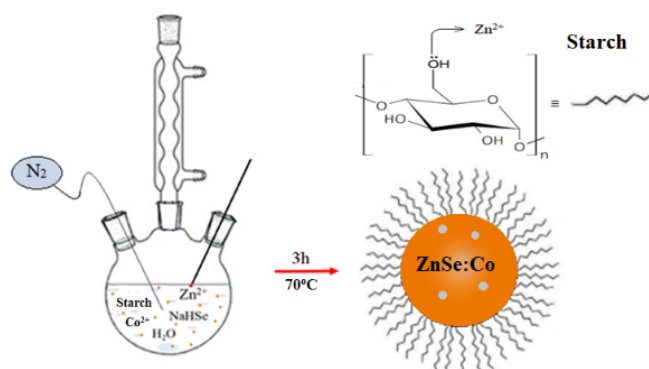
2. EXPERIENCE

2.1 Materials

Zinc acetate dihydrate (Zn(CH₃COO)₂·2H₂O), cobalt acetate tetrahydrate (Co(CH₃COO)₂·4H₂O), sodium hydrogen selenide (NaHSe), starch (as a stabilizer), ammonium hydroxide (NH₄OH), and deionized water were used as starting materials for the synthesis of ZnSe:Co quantum dots (QDs). All reagents were of analytical grade and used without further purification.

2.2 Synthesis ZnSe: Co-Starch QDs

Co²⁺-doped ZnSe quantum dots (QDs) were synthesized using an aqueous chemical precipitation method with starch as a stabilizing agent to prevent nanoparticle aggregation. A 250 mL round-bottom flask was used to mix 15 mL of Zn²⁺ solution with varying volumes of Co²⁺ solution (corresponding to different doping concentrations). To enhance dispersion and control particle growth, 50 mL of 0.1N starch solution and 90 mL of deionized water were added, and the mixture was stirred for 15 minutes to ensure homogeneity. The pH of the solution was carefully adjusted to 10 using 2M NH₄OH, as this pH level was optimized to stabilize metal precursors, prevent Zn(OH)₂ precipitation, and reduce defect-related recombination centers. The reaction temperature gradually increased to 70°C, which was identified as the optimal temperature for controlled nucleation and growth of ZnSe:Co QDs. Lower temperatures (<50°C) resulted in incomplete nucleation and polydisperse QDs, whereas higher temperatures (>80°C) led to rapid particle growth, diminishing quantum confinement effects. Once the system stabilized at 70°C, the NaHSe solution was added dropwise, initiating QD formation. The reaction was maintained for 3 hours, as this duration allowed for adequate crystal growth while preserving nanoscale properties. Shorter reaction times (<1 hour) led to defect-rich, underdeveloped QDs with weak fluorescence, while longer reaction times (>5 hours) caused excessive particle aggregation, reducing the quantum confinement effect. Upon completion, the synthesized ZnSe:Co QDs were collected via centrifugation at 10,000 rpm for 15 minutes, followed by multiple washing steps with deionized water and ethanol to remove unreacted precursors and byproducts. The purified QDs were then dried at 60°C under a vacuum for further characterization.



Scheme 1. Synthesis of ZnSe:Co Starch

2.3 Characteristics of ZnSe:Co Starch QDs

Using spectroscopic techniques, the structural, optical, and compositional properties of ZnSe:Co Starch quantum dots were comprehensively analyzed. The crystallographic structure and phase purity of the samples were analyzed using an X-ray diffractometer (XRD) (Bruker D8 Advance, Cu K α radiation, $\lambda = 0.15406$ nm, 40 kV, 40 mA, scan range 20°–80°). The elemental composition and doping efficiency of Co²⁺ in ZnSe QDs were examined using EDX analysis (Oxford Instruments, model X-MaxN, 20 kV accelerating voltage, SEM mode). The optical bandgap and quantum confinement effects were studied using a Shimadzu UV-2600 spectrophotometer (range: 200–800 nm, scan speed: 200 nm/min, quartz cuvette, 1 cm path length). Emission characteristics and defect-related transitions were analyzed using a Fluorescence Spectrometer (Horiba FluoroMax-4, excitation wavelength: 325 nm, emission range: 350–750 nm, slit width: 2 nm). Surface functional groups and interaction between ZnSe QDs and starch stabilizer were identified using FTIR spectroscopy (Bruker Vertex 70, range: 4000–500 cm⁻¹, resolution: 4 cm⁻¹, ATR mode). The oxidation states and chemical environment of Zn, Se, and Co were determined using XPS (Thermo Fisher ESCALAB 250Xi, monochromatic Al K α source, 1486.6 eV, pass energy: 20 eV for high-resolution scans). Morphology, particle size distribution, and crystallinity were examined using STEM (JEOL JEM-2100F, accelerating voltage: 200 kV, bright-field and dark-field imaging modes). SAED patterns were recorded to confirm the phase purity of the ZnSe:Co QDs. The magnetic properties were analyzed using a Vibrating Sample Magnetometer (VSM, Lakeshore 7404, temperature: 300 K, applied field: ± 1.5 T) to measure hysteresis loops and saturation magnetization (M_s).

3. RESULTS AND DISCUSSION

Figure 1a shows the X-ray diffraction (XRD) patterns of the undoped and Co-doped ZnSe QDs with varying concentrations. Figure 1a shows that all samples exhibit diffraction peaks at 2θ angles of approximately 25.69°, 27.12°, 27.09°, 37.96°, 45.58°, 49.51°, 53.78°, 60.58°, and 69.58° corresponding to the lattice planes (100), (002), (101), (102), (110), (103), (112), (202), and (203), respectively, corresponding to the hexagonal wurtzite ZnSe structure. The XRD patterns of the obtained samples match those of ZnSe (JCPDS# 15-0105). Notably, no additional peaks corresponding to Co metal or secondary Co-based phases were observed, indicating successful Co incorporation into the ZnSe lattice.

To further examine the crystalline and phase purity, SAED analysis was performed (Figure 1b). The SAED pattern displays a series of concentric diffraction rings, characteristic of nanocrystalline materials. These diffraction rings correspond to the expected lattice planes of wurtzite ZnSe [19, 20], further validating the XRD results. It is important to note that individual ZnSe:Co QDs are single-crystalline, but since multiple QDs are illuminated within the electron

diffraction aperture, the ensemble produces a polycrystalline-like diffraction pattern. This observation does not indicate that the QDs themselves are polycrystalline but rather reflects the diffraction contributions from multiple nanoscale crystallites within the selected area. The combination of XRD and SAED confirms that the ZnSe:Co QDs maintain high crystallinity and phase purity, with Co^{2+} incorporation inducing minimal structural distortion.

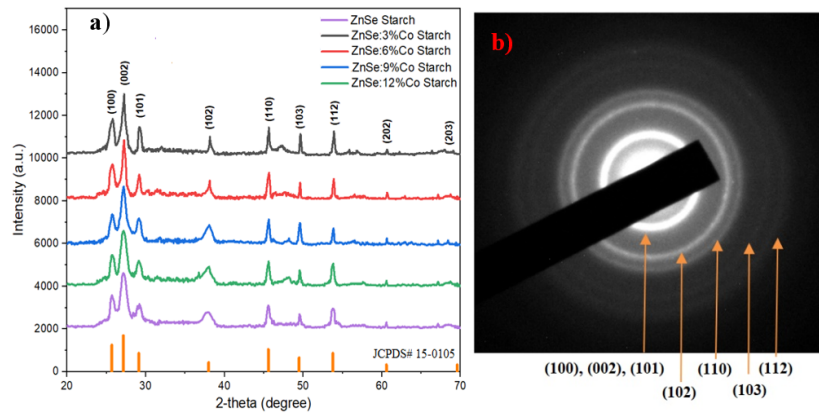


Figure 1. a) The XRD results of ZnSe:Co Starch at 70 °C with various $\text{Co}^{2+}/\text{Zn}^{2+}$ ratios and b) SEAD of ZnSe:9%Co Starch

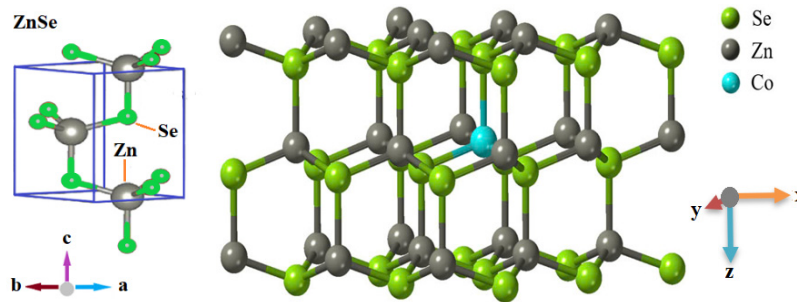


Figure 2. Illustrations of the unit cell and crystal structure of ZnSe:Co.

The ZnSe:Co unit cells and crystal structures are shown in Figure 2. The unit cell of hexagonal ZnSe (Figure 2) and Co-doped ZnSe crystal structure (Figure 2) are best illustrated using the VESTA visualization tool using experimentally determined parameters, which are also shown in Table 1. Equations (1) – (3) [21, 22] were used to compute the lattice parameters a , c , and the cell volume, which are listed in Table 1.

$$d_{hkl} = \frac{K\lambda}{\beta \cos \theta} \quad (1)$$

where d is the average crystallite size, β is the full width at half maximum (FWHM) of the peaks, λ is the well-known X-ray wavelength (0.15406 nm), K is a constant assumed to be 0.9, θ is the angle of Bragg diffraction, and the Miller index of the crystal plane is (hkl) .

Using the XRD pattern and Equation (2), the lattice parameters a and c of the hexagonal structure were computed and are listed in Table 1.

$$\frac{1}{d_{hkl}^2} = \frac{4}{3} \left(\frac{h^2 + hk^2 + k^2}{a^2} \right) + \frac{l^2}{c^2} \quad (2)$$

Lattice constants a and c were computed for the (100) and (002) planes, respectively. The volume (V) of the unit cell of the hexagonal system was computed using Equation (3):

$$V = \frac{\sqrt{3}}{2} c \cdot a^2 \quad (3)$$

Table 1. Concentration-dependent average semiconductor nanocrystal size, lattice properties, and unit cell volume

Sample Name	d (nm)	a (Å)	c (Å)	c/a (Å)	Volume, V (Å ³)
ZnSe-Starch	7.22	3.995	6.557	1.641	90.61
ZnSe:3%Co Starch	6.72	3.992	6.552	1.641	90.41
ZnSe:6%Co Starch	6.33	3.987	6.547	1.642	90.14
ZnSe:9%Co Starch	5.02	3.984	6.545	1.643	89.97
ZnSe:12%Co Starch	4.90	3.986	6.542	1.641	90.00

The parameters that were determined are listed in Table 1. The addition of Co to the ZnSe lattice alters the lattice parameters a and c of the ZnSe:Co QDs. As the concentration of Co increased, the lattice parameters a , c , c/a , and the cell

volume decreased. The results revealed a decrease in the lattice constants (a and c) with increasing Co doping concentration, attributed to the substitution of Zn^{2+} ions (ionic radius: 0.74 \AA) with smaller Co^{2+} ions (ionic radius: 0.72 \AA). These findings establish a direct relationship between doping concentration and structural modifications in ZnSe QDs, providing valuable insights for tuning their physical properties for specific applications. In addition, the c/a ratio remained consistent with the ideal wurtzite structure, confirming the structural integrity of the ZnSe lattice despite the doping.

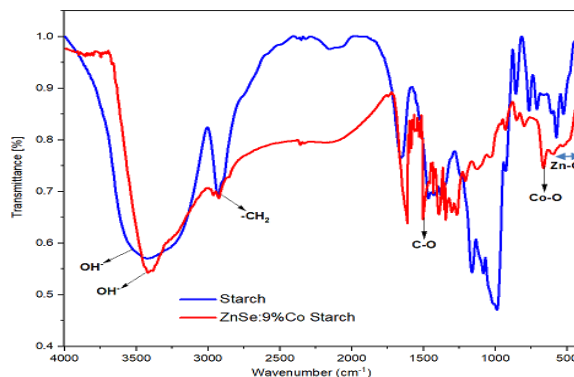


Figure 3. FT-IR spectra of Starch and ZnSe:9%Co Starch QDs

The FT-IR spectra of the starch paste and ZnSe:9%Co Starch sample (Figure 3). This figure shows that the vibration peaks of -OH, C-C, -CH₂, and -CO of starch paste still exist, proving that a bond has been formed on the surface between ZnSe crystals and starch paste, and the starch paste was bonded with QDs particles. This increases its capacity to diffuse in water, making it more suitable for biological applications because it is compatible with biological cells [22]. Figure 3 shows that the vibration peaks corresponding to the wavenumber 3405 cm^{-1} are characteristic vibrations of the -O-H bond of starch [25, 26]. The width of the vibration peak is attributed to the formation of hydrogen bonds [25], and the peak at 1650 cm^{-1} is characteristic of the -O-H bond of water adsorbed on the material surface [26]. The 1156 cm^{-1} peak corresponds to the C-O bond of the C-O-H group. The peak at 2895 cm^{-1} corresponds to the asymmetric C-H bond [25]. The peaks that correspond to the wavenumbers at 1020 cm^{-1} and 1417 cm^{-1} are indicative of the C-O bond of the C-O-C and C-C groups in the anhydrous glucose ring, respectively [27,28]. The vibrational peak at 992 cm^{-1} corresponds to the α 1-4 glycosidic (C-O-O) vibration. The Zn-O absorption band at 400 to 600 cm^{-1} is attributed to Zn-O [29–32]. The peak at $671,2 \text{ cm}^{-1}$ corresponded to stretching vibrational modes of Co-O in ZnSe:9%Co Starch QDs [33]. The C-C bond was identified by the vibrational peak at 757 cm^{-1} , which corresponds to the wavenumber [25]. Therefore, the -OH, C-C, -CH₂, and -CO vibration peaks of the starch paste were still present at the same time, indicating the development of a link between the ZnSe crystals and the starch paste on the surface. This makes them more friendly to biological cells, improves their dispersion in water, and aids beneficial biological applications [22].

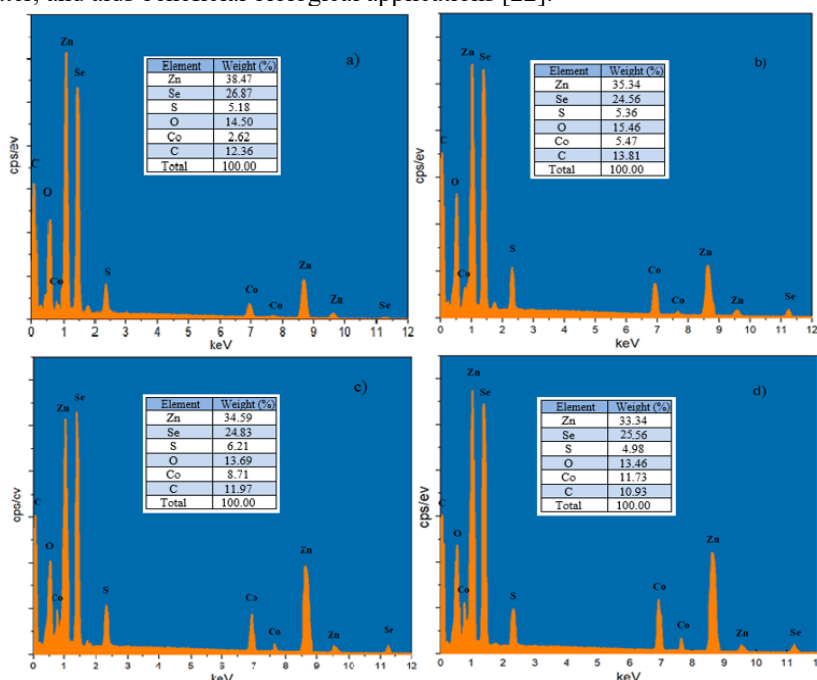


Figure 4. EDX spectra of Co-doped ZnSe QDs with various $\text{Co}^{2+}/\text{Zn}^{2+}$ ratio: (a) ZnSe:3%Co Starch, (b) ZnSe:6%Co Starch, (c) ZnSe:9%Co Starch, (d) ZnSe:12%Co Starch

EDX spectroscopy was employed to validate the elemental composition of ZnSe:Co QDs (Figure 4). The spectra (Figure 4a, b, c, d) revealed the presence of Zn, Se, and Co, along with carbon and oxygen from the starch stabilizer. As the Co doping concentration increased, the proportion of Co ions incorporated into the ZnSe matrix correspondingly increased. However, the measured Co/Zn ratio was slightly lower than the theoretical value, suggesting partial loss of Co ions during the synthesis and washing processes. The consistent absence of unexpected elements confirmed the high purity of the synthesized QDs. In addition, an even distribution of elements within the samples was observed, further supporting the successful integration of Co ions into the ZnSe lattice.

Figure 5 shows the energy-dispersive X-ray spectrum (EDS) of ZnSe:Co Starch obtained using scanning transmission electron microscopy (STEM). Zn and Se atoms were found throughout the particles. The presence of Co, O, and C in ZnSe:Co Starch has also been established.

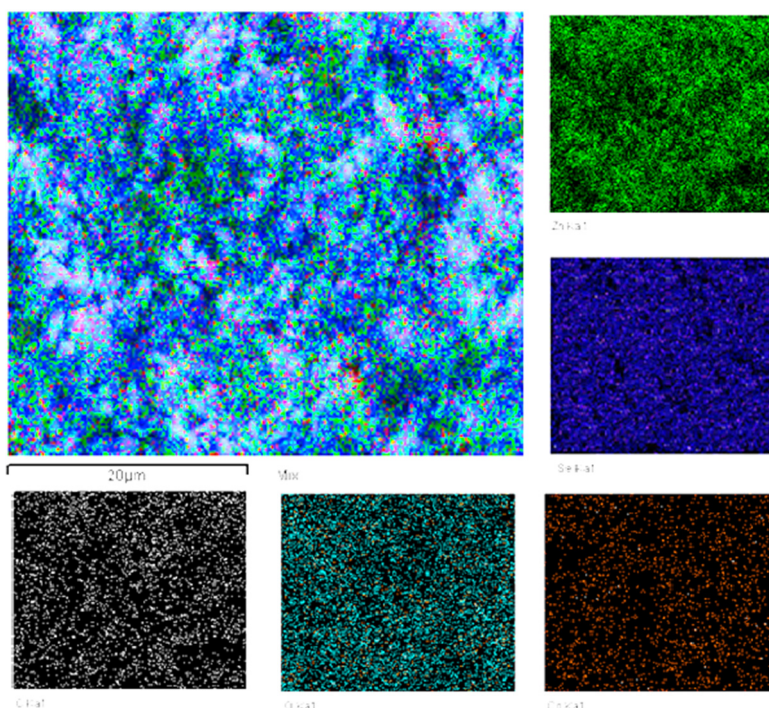


Figure 5. EDS-STEM image of the ZnSe:9%Co Starch particles

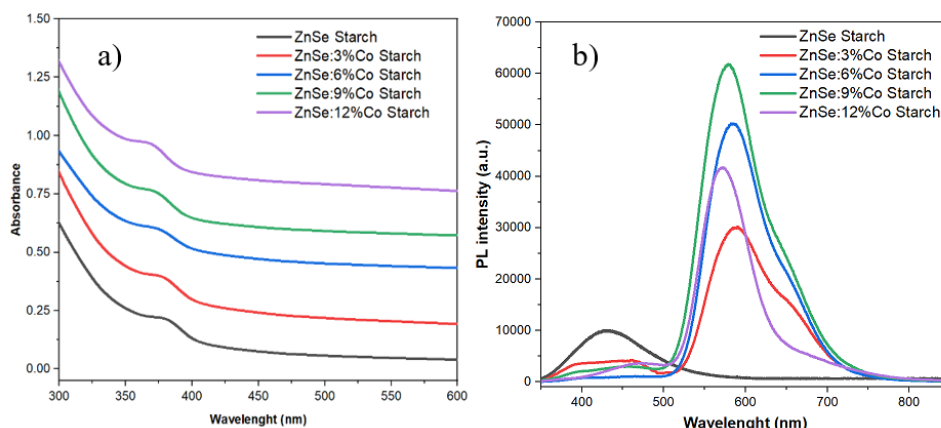


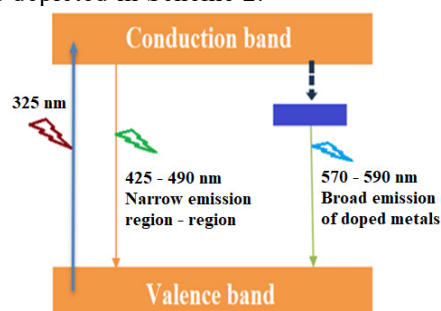
Figure 6. a) UV-Vis spectrum and b) photoluminescence of ZnSe Starch, ZnSe:Co Starch (3, 6, 9 and 12%) QDs synthesized at 70°C, pH 10

Figure 6a shows the absorption spectrum of ZnSe:Co Starch QDs. The UV-visible absorption spectra of the ZnSe:Co QDs displayed distinct blue shifts in the excitonic absorption peak with increasing Co^{2+} doping concentration. The initial absorption peak of the undoped ZnSe QDs was observed at 387 nm, corresponding to an energy of 3.16 eV. This energy is significantly higher than that of the bulk ZnSe bandgap (2.75 eV) owing to quantum confinement effects. As the Co doping concentration increased from 3% to 12%, the absorption peak shifted to shorter wavelengths, indicating a decrease in the particle size. This blue shift and reduction in size are consistent with the substitution of Zn^{2+} ions by smaller Co^{2+} ions, which affects the lattice structure and enhances quantum confinement [34,35]. The photoluminescence spectra of the ZnSe:Co QDs (Figure 6b) exhibited two distinct emission peaks: a high-energy peak at approximately 435 nm and a

broad, long-wavelength peak around 579 nm. The high-energy peak corresponds to band-to-band recombination in ZnSe, whereas the broader emission at 579 nm is attributed to defect states and Co-related transitions within the doped lattice. The intensity of the PL emission strongly depended on the Co doping concentration. At lower doping levels (3%), the intensity of the Co-related emission peak is relatively weak, indicating fewer Co-related defect states. As the doping concentration increased to 6% and 9%, the intensity of the long-wavelength emission peak increased significantly, reaching a maximum of 9%. This enhancement is attributed to the increased number of Co^{2+} ions substituting Zn^{2+} ions in the lattice, creating more Co-related defect centers that act as luminescent centers.

However, when the Co doping concentration exceeded 9%, the intensity of the Co-related emission decreased. This quenching effect is likely due to Co-Co interactions, which lead to the formation of nonradiative recombination pathways, reducing the overall fluorescence efficiency. In addition, spin-spin coupling between Co^{2+} ions at higher concentrations may further suppress luminescence. These observations highlight the delicate balance between the doping concentration and optical properties. An optimal doping concentration of 9% achieved the highest luminescence efficiency, making it the most suitable for applications requiring strong emission properties. The results confirm that Co^{2+} doping significantly influences the optical characteristics of ZnSe QDs by modulating the defect states and luminescence behavior of the material.

The presence of Co^{2+} ions in the crystal field of ZnSe resulted in distinct energy levels in the bandgap. Under the effect of the crystal field and spin-orbit interactions, the energy levels are divided into distinct sub-energy levels [36]. This result once again proves that Co^{2+} ions enter the ZnSe matrix and replace the Zn ions. The energy-level diagram of the Co-doped ZnSe QDs is depicted in Scheme 2.



Scheme 2. Energy band diagram and emission mechanisms of Co-doped ZnSe QDs

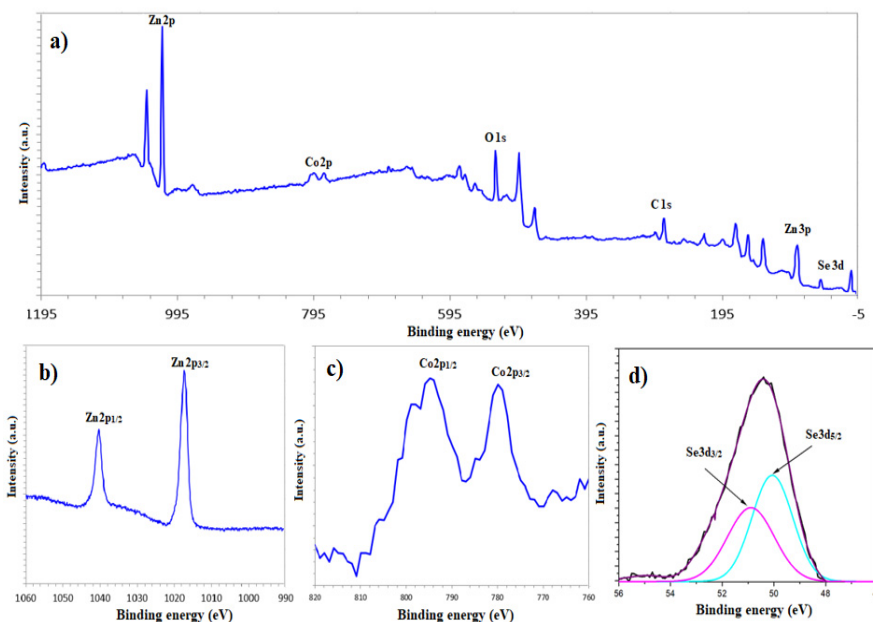


Figure 7. XPS spectrum of ZnSe:9%Co-starch, (b) Zn 2p peak, (c) Co 2p peak, and (d) Se3d peak.

XPS analysis (Figure 7) was employed to determine the elemental composition and chemical states of the ZnSe:Co QDs. The survey spectrum confirms the presence of Zn, Se, Co, O, and C in the doped QDs. High-resolution spectra (Figure 7a) provide further insight into the chemical environment of the elements. The Zn 2p peaks (Figure 7b) were observed at binding energies of 1021.6 eV (Zn 2p_{3/2}) and 1044.8 eV (Zn 2p_{1/2}), consistent with Zn in the +2-oxidation state [37–39]. The peak at 527.3 eV corresponds to the binding energy of O 1s. For Co, the Co 2p_{3/2} and Co 2p_{1/2} peaks (Figure 7c) were observed at 780.1 eV and 795.8 eV, respectively, indicating the presence of Co in the +2 oxidation state [38,39]. Additionally, satellite peaks in the Co 2p region confirmed the high-spin state of the Co^{2+} ions. The Se 3d peaks in Figure 7d can be separated into two overlapping peaks, Se 3d_{5/2} and Se 3d_{3/2}, at binding energies of 50.2 eV and

51.5 eV, respectively, reflecting Se 3d in Zn-Se. The XPS results strongly support the successful doping of Co^{2+} ions into the ZnSe lattice and their interactions with the crystal matrix. These findings align with the structural and optical analyses, reinforcing the multifunctional nature of ZnSe:Co QDs.

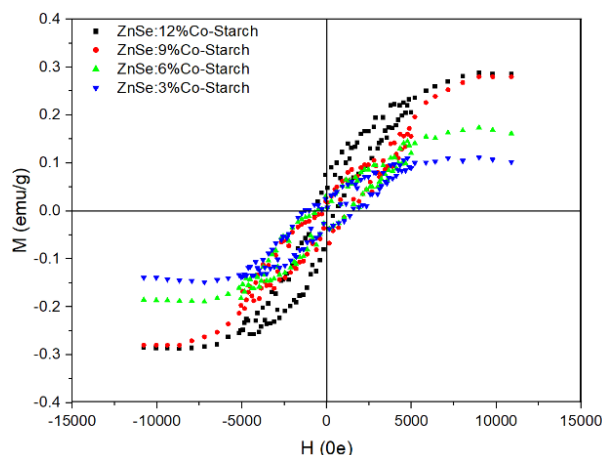


Figure 8. Hysteresis curves of ZnSe:3%Co Starch, ZnSe:6%Co Starch, ZnSe:9%Co Starch, and ZnSe:12%Co Starch QDs

The magnetic properties of the ZnSe:Co QDs were investigated using magnetic hysteresis measurements, which revealed clear evidence of ferromagnetic behavior at room temperature (Figure 8). The saturation magnetization (“Ms”) of the Co-doped ZnSe QDs increased with Co^{2+} doping concentration, reaching a maximum value at 12% Co^{2+} doping. Specifically, the Ms values recorded were 0.112, 0.174, 0.280, and 0.288 emu/g for samples with Co^{2+} doping concentrations of 3%, 6%, 9%, and 12%, respectively. The magnetic properties of the Co-doped ZnSe QDs can be explained by the exchange interaction between the Co^{2+} ions and the substrate lattice. The half-filled 3D shell of Co^{2+} can contribute to sp^3 bonding and substitute for Zn ions, resulting in local spin in the dilute magnetic semiconductors of the $\text{A}_{\text{II}}\text{B}_{\text{VI}}$ group [42]. Co^{2+} in the $\text{A}_{\text{II}}\text{B}_{\text{VI}}$ group semiconductor compounds is divalent, resulting in a high-spin configuration d^5 .

At lower doping levels, the interaction between the Co^{2+} ions was relatively weak, resulting in moderate magnetization. As the Co^{2+} concentration increased, stronger exchange interactions occurred, which enhanced the overall magnetic moment. However, at higher doping levels, such as 12%, saturation of Ms was observed, indicating a potential limit for the effective incorporation of Co^{2+} ions into the ZnSe lattice. Beyond this concentration, Co clustering or the formation of secondary phases may contribute to changes in magnetic behavior, limiting further increases in magnetization. This demonstrates that Co doping imparts ferromagnetic properties to ZnSe QDs and enables the precise tuning of their magnetic characteristics by controlling the Co^{2+} concentration. The combination of optical and magnetic properties makes Co-doped ZnSe QDs promising candidates for application in spintronics, magnetic memory devices, and multifunctional nanomaterials.

4. CONCLUSIONS

Co-doped ZnSe QDs with molar ratios of $\text{Co}^{2+}/\text{Zn}^{2+}$ ranging from 3-12% were produced with a wurtzite structure and a size of 5-7 nm. Co-doping of the ZnSe matrix did not modify the matrix structure but diminished the crystal lattice constant and grain size as the Co^{2+} concentration increased. As the Co^{2+} concentration rises, more Co^{2+} ions with a smaller radius (0.72 Å) are substituted for Zn^{2+} ions with a larger radius (0.74 Å) in ZnSe, which results in a decrease in the lattice constant. As the Co concentration rises from 3-12%, the absorption and fluorescence maxima from 4-16 nm likewise shifted blue owing to the shrinkage of the ZnSe: Co QDs. The PL spectra of the Co-doped ZnSe QDs showed two peaks at short wavelengths (approximately 435 nm) and long wavelengths (approximately 579 nm), corresponding to Co^{2+} concentrations ranging from 3-12%, whereas the emission intensity at short wavelengths decreased and increased. This phenomenon can be explained by the fact that as the concentration of Co^{2+} increased, so did the substitution of Co^{2+} by Zn^{2+} . Co-doped ZnSe QDs are ferromagnetic. The saturation magnetization values of the Co-doped ZnSe QDs at concentrations of 3, 6, 9, and 12% were 0.112, 0.174, 0.280, and 0.288 emu/g, respectively. The magnetism of Co-doped ZnSe QDs is induced by an exchange contact between Co^{2+} ions and the matrix or by Co cluster formation.

Authors’ Contributions: Thi-Diem Bui: Methodology, Validation, Project administration. Van Cuong Nguyen: Investigation, Trong Tang Nguyen: Resources. Phuc Huu Dang: Writing, review, and editing. Quang-Liem Nguyen: Writing - review & editing, Funding Not applicable

Availability of data and material Not applicable.

Declarations

Ethical Approval Not applicable.

Consent to Participate Not applicable.

Consent for Publication: Not applicable.

Competing Interest: The authors have no competing interest to declare

ORCID

Thi Diem Bui, <https://orcid.org/0000-0003-3668-1496>; Quang-Liem Nguyen, <https://orcid.org/0000-0003-1804-5031>

Trong Tang Nguyen, <https://orcid.org/0000-0002-3706-1048>; Huu Phuc Dang, <https://orcid.org/0000-0002-8982-0421>

REFERENCES

- [1] S.B. Singh, M.V. Limaye, S.K. Date, *et al.* "Iron substitution in CdSe nanoparticles: Magnetic and optical properties," *Phys. Rev. B*, **80**(23), 235421 (2009). <https://doi.org/10.1103/physrevb.80.235421>
- [2] H.T. Van, N.D. Vinh, N.X. Ca, *et al.* "Effects of ligand and chemical affinity of S and Se precursors on the shape, structure and optical properties of ternary CdS_{1-x}Sex alloy nanocrystals," *Mater. Lett.* **264**, 127387 (2020). <https://doi.org/10.1016/j.matlet.2020.127387>
- [3] N.X. Ca, H.T. Van, P.V. Do, *et al.* "Influence of precursor ratio and dopant concentration on the structure and optical properties of Cu-doped ZnCdSe-alloyed quantum dots," *RSC Adv.* **10**(43), 25618–25628 (2020). <https://doi.org/10.1039/d0ra04257a>
- [4] S. Das, and K.C. Mandal, "Optical downconversion in rare earth (Tb³⁺ and Yb³⁺) doped CdS nanocrystals," *Mater. Lett.* **66**(1), 46–49 (2012). <https://doi.org/10.1016/j.matlet.2011.08.034>
- [5] K. Senthilkumar, T. Kalaivani, S. Kanagesan, *et al.* "Synthesis and characterization studies of ZnSe quantum dots," *Journal of Materials Science: Materials in Electronics*, **23**(11), 2048–2052 (2012). <https://doi.org/10.1007/s10854-012-0701-1>
- [6] U.B. Memon, U. Chatterjee, M.N. Gandhi, *et al.* "Synthesis of ZnSe Quantum Dots with Stoichiometric Ratio Difference and Study of its Optoelectronic Property," *Procedia Materials Science*, **5**, 1027–1033 (2014). <https://doi.org/10.1016/j.mspro.2014.07.393>
- [7] F. Baum, M.F. da Silva, G. Linden, *et al.* "Growth dynamics of zinc selenide quantum dots: the role of oleic acid concentration and synthesis temperature on driving optical properties," *Journal of Nanoparticle Research*, **21**(2), 42 (2019). <https://doi.org/10.1007/s11051-019-4485-6>
- [8] N.R. Vempuluru, H. Kwon, R. Parnapalle, *et al.* "ZnS/ZnSe heterojunction photocatalyst for augmented hydrogen production: Experimental and theoretical insights," *Int. J. Hydrogen Energy*, **51**, 524–539 (2024). <https://doi.org/10.1016/j.ijhydene.2023.08.249>
- [9] S. Lin, J. Li, C. Pu, *et al.* "Surface and intrinsic contributions to extinction properties of ZnSe quantum dots," *Nano Res.* **13**(3), 824–831 (2020). <https://doi.org/10.1007/s12274-020-2703-2>
- [10] T. Zahra, M.M. Alanazi, S.D. Alahmari, *et al.* "Hydrothermally synthesized ZnSe@FeSe nanocomposite: A promising candidate for energy storage devices," *Int. J. Hydrogen Energy*, **59**, 97–106 (2024). <https://doi.org/10.1016/j.ijhydene.2024.01.293>
- [11] M. El-Assar, T.E. Taha, F.E.A. El-Samie, *et al.* "ZnSe-based highly-sensitive SPR biosensor for detection of different cancer cells and urine glucose levels," *Opt. Quantum Electron.* **55**, 76 (2023). <https://doi.org/10.1007/s11082-022-04326-y>
- [12] N.T. Hien, P.M. Tan, H.T. Van, *et al.* "Photoluminescence properties of Cu-doped CdTeSe alloyed quantum dots versus laser excitation power and temperature," *J. Lumin.* **218**, 116838 (2020). <https://doi.org/10.1016/j.jlumin.2019.116838>
- [13] N.X. Ca, N.T. Hien, P.N. Loan, *et al.* "Optical and Ferromagnetic Properties of Ni-Doped CdTeSe Quantum Dots," *J. Electron. Mater.* **48**(4), 2593–2599 (2019). <https://doi.org/10.1007/s11664-019-07017-9>
- [14] N.A. Hamizi, F. Aplop, H.Y. Haw, *et al.* "Tunable optical properties of Mn-doped CdSe quantum dots synthesized via inverse micelle technique," *Opt. Mater. Express*, **6**(9), 2915 (2016). <https://doi.org/10.1364/ome.6.002915>
- [15] H.T. Van, N.D. Vinh, P.M. Tan, *et al.* "Synthesis and optical properties of tunable dual emission copper doped CdTe_{1-x}Sex alloy nanocrystals," *Opt. Mater. (Amst)*, **97**, 109392 (2019). <https://doi.org/10.1016/j.optmat.2019.109392>
- [16] A. Ganguly, and S.S. Nath, "Mn-doped CdS quantum dots as sensitizers in solar cells," *Materials Science and Engineering: B*, **255**, 114532 (2020). <https://doi.org/10.1016/j.mseb.2020.114532>
- [17] F. Ibraheem, M.A. Mahdy, E.A. Mahmoud, *et al.* "Tuning Paramagnetic effect of Co-Doped CdS diluted magnetic semiconductor quantum dots," *J. Alloys Compd.* **834**, 155196 (2020). <https://doi.org/10.1016/j.jallcom.2020.155196>
- [18] S. Xiong, B. Xi, C. Wang, *et al.* "Solution-Phase Synthesis and High Photocatalytic Activity of Wurtzite ZnSe Ultrathin Nanobelts: A General Route to 1D Semiconductor Nanostructured Materials." *Chemistry – A European Journal*, **13**(28), 7926–7932 (2007). <https://doi.org/10.1002/chem.200700334>
- [19] T. Gupta, and R.P. Chauhan, "Structural, morphological, and electrical properties of ZnSe nanostructures: Effects of Zn precursors," *Surfaces and Interfaces*, **25**, 101196 (2021). <https://doi.org/10.1016/j.surfin.2021.101196>
- [20] R.K. Yadav, and P. Chauhan, "Estimation of lattice strain in Mn-doped ZnO nanoparticles and its effect on structural and optical properties," *Indian Journal of Pure & Applied Physics*, **57**, 881–890 (2019). <https://nopr.niscair.res.in/bitstream/123456789/52775/1/IJPAP%2057%2812%29%20881-890.pdf>
- [21] R. Khalid, A.N. Alhazaa, and M.A.M. Khan, "Synthesis, characterization and properties of Mn-doped ZnO nanoparticles," *Applied Physics A*, **124**(8), 536 (2018). <https://doi.org/10.1007/s00339-018-1934-5>
- [22] M.T. Yarak, M. Tayebi, M. Ahmadi, *et al.* "Synthesis and optical properties of cysteamine-capped ZnS quantum dots for aflatoxin quantification," *J. Alloys Compd.* **690**, 749–758 (2017). <https://doi.org/10.1016/j.jallcom.2016.08.158>
- [23] F. Iselau, T.P. Xuan, A. Matic, *et al.* "Competitive adsorption of amylopectin and amylose on cationic nanoparticles: a study on the aggregation mechanism," *Soft Matter*, **12**(14), 3388–3397 (2016). <https://doi.org/10.1039/c6sm00165c>
- [24] O.S. Oluwafemi, and O.O. Adeyemi, "One-pot room temperature synthesis of biopolymer-capped ZnSe nanoparticles," *Mater. Lett.* **64**(21), 2310–2313 (2010). <https://doi.org/10.1016/j.matlet.2010.07.021>
- [25] K. Senthilkumar, T. Kalaivani, S. Kanagesan, *et al.* "Low temperature method for synthesis of starch-capped ZnSe nanoparticles and its characterization studies," *J. Appl. Phys.* **112**(11), (2012). <https://doi.org/10.1063/1.4767924>
- [26] M. Grabolle, M. Spieles, V. Lesnyak, *et al.* "Determination of the Fluorescence Quantum Yield of Quantum Dots: Suitable Procedures and Achievable Uncertainties," *Anal. Chem.* **81**(15), 6285–6294 (2009). <https://doi.org/10.1021/ac900308v>
- [27] N. Soltani, E. Saion, W.M.M. Yunus, *et al.* "Enhancement of visible light photocatalytic activity of ZnS and CdS nanoparticles based on organic and inorganic coating," *Appl. Surf. Sci.* **290**, 440–447 (2014). <https://doi.org/10.1016/j.apsusc.2013.11.104>
- [28] I. Elhamdi, H. Souissi, O. Taktak, *et al.* "Experimental and modeling study of ZnO:Ni nanoparticles for near-infrared light emitting diodes," *RSC Adv.* **12**(21), 13074–13086 (2022). <https://doi.org/10.1039/d2ra00452f>

- [29] A. Sahai, and N. Goswami, "Structural and vibrational properties of ZnO nanoparticles synthesized by the chemical precipitation method," *Physica E: Low Dimens. Syst. Nanostruct.* **58**, 130–137 (2014). <https://doi.org/10.1016/j.physe.2013.12.009>
- [30] R. Yuvakkumar, J. Suresh, B. Saravanakumar, et al. "Rambutan peels promoted biomimetic synthesis of bioinspired zinc oxide nanochains for biomedical applications," *Spectrochim Acta A: Mol. Biomol. Spectrosc.* **137**, 250–258 (2015). <https://doi.org/10.1016/j.saa.2014.08.022>
- [31] R.F. Silva, and M.E.D. Zaniquelli, "Morphology of nanometric size particulate aluminium-doped zinc oxide films," *Colloids Surf. A: Physicochem. Eng. Asp.* **198–200**, 551–558 (2002). [https://doi.org/10.1016/S0927-7757\(01\)00959-1](https://doi.org/10.1016/S0927-7757(01)00959-1)
- [32] K.M. Gendo, R.F. Bogale, and G. Kenasa, "Green Synthesis, Characterization, and Evaluation of Photocatalytic and Antibacterial Activities of Co₃O₄-ZnO Nanocomposites Using *Calpurnia aurea* Leaf Extract," *ACS Omega*, **9**(26), 28354–28371 (2024). <https://doi.org/10.1021/acsomega.4c01595>
- [33] L. Liu, L. Yang, Y. Pu, et al. "Optical properties of water-soluble Co²⁺/ZnS semiconductor nanocrystals synthesized by a hydrothermal process," *Mater. Lett.* **66**(1), 121–124 (2012). <https://doi.org/10.1016/j.matlet.2011.08.025>
- [34] S. Sambasivam, D.P. Joseph, J.G. Lin, et al. "Doping induced magnetism in Co–ZnS nanoparticles," *J. Solid State Chem.* **182**(10), 2598–2601 (2009). <https://doi.org/10.1016/j.jssc.2009.07.015>
- [35] G. Murugadoss, B. Rajamannan, and V. Ramasamy, "Synthesis and Photoluminescence Study Of PVA-Capped ZnS:Mn²⁺ Nanoparticles, Dig. J. Nanomater. Biostruct. **991**(1–3), 202–206 (2010). <https://doi.org/10.1016/j.molstruc.2011.02.026>
- [36] F. Qiao, R. Kang, Q. Liang, et al. "Tunability in the Optical and Electronic Properties of ZnSe Microspheres via Ag and Mn Doping," *ACS Omega*, **4**(7), 12271–12277 (2019). <https://doi.org/10.1021/acsomega.9b01539>
- [37] G.M. Lohar, H.D. Dhaygude, R.A. Patil, et al. "Studies of properties of Fe²⁺ doped ZnSe nano-needles for photoelectrochemical cell application," *Journal of Materials Science: Materials in Electronics.* **26**(11), 8904–8914 (2015). <https://doi.org/10.1007/s10854-015-3572-4>
- [38] C. Li, H. Zhang, and C. Cheng, "CdS/CdSe co-sensitized 3D SnO₂/TiO₂ sea urchin-like nanotube arrays as an efficient photoanode for photoelectrochemical hydrogen generation," *RSC Adv.* **6**(44), 37407–37411 (2016). <https://doi.org/10.1039/c6ra02176j>
- [39] S. Laureti, E. Agostinelli, G. Scavia, et al. "Effect of oxygen partial pressure on PLD cobalt oxide films," *Appl. Surf. Sci.* **254**(16), 5111–5115 (2008). <https://doi.org/10.1016/j.apsusc.2008.02.055>
- [40] X. Su, L. Wang, J. Chen, et al. "Role of cobalt in ZnO:Co thin films," *J. Phys. D Appl. Phys.* **44**(26), 265002 (2011). <https://doi.org/10.1088/0022-3727/44/26/265002>
- [41] N.F. Djaja, D.A. Montja, and R. Saleh, "The Effect of Co Incorporation into ZnO Nanoparticles. Advances in Materials Physics and Chemistry," **03**(01), 33–41 (2013). <https://doi.org/10.4236/ampc.2013.31006>

ФОТОЛЮМІНЕСЦЕНЦІЯ ТА МАГНІТНЕ ПІДСИЛЕННЯ В КВАНТОВИХ ТОЧКАХ ZnSe ЧЕРЕЗ КЕРОВАНЕ ЛЕГУВАННЯ КОБАЛЬТОМ

Тхі Дьєм Буй¹, Куанг-Лієм Нгуєн², Ван Куонг Нгуєн¹, Тронг Танг Нгуєн¹, Хуу Фук Данг³

¹Факультет хімічної інженерії, Індустріальний університет Хошіміна, Хошімін, В'єтнам

²Інститут матеріалознавства, В'єтнамська академія наук і технологій, Ханой, В'єтнам

³Факультет фундаментальних наук, Індустріальний університет Хошіміна, Хошімін, В'єтнам

Квантові точки (КТ) напівпровідників ZnSe, леговані іонами Co²⁺, були синтезовані у водному розчині з використанням крохмалю як поверхневого стабілізатора для забезпечення дисперсії наночастинок. Структурний та композиційний аналізи з використанням рентгенівської дифракції (XRD) та енергодисперсійної рентгенівської спектроскопії (EDX) підтвердили успішне включення іонів Co²⁺ у матрицю ZnSe. Для визначення кристалічної структури, параметрів решітки та розмірів частинок квантових точок ZnSe, легованих Co, були використані рентгенівська дифракція та УФ-видима абсорбційна спектроскопія. Оптичні властивості були проаналізовані за допомогою абсорбційної та флуоресцентної спектроскопії, яка виявила зсув піку поглинання до синього кольору зі збільшенням концентрації Co через ефекти квантового обмеження та зміни розміру частинок. Аналіз фотолюмінесценції (PL) виявив подвійні піки випромінювання, що відповідають міжзонній рекомбінації та дефектним станам, пов'язаним з Co, з максимальною ефективністю люмінесценції, що спостерігається при рівні легування 9% Co. Поза цією концентрацією ефекти гасіння, пов'язані з взаємодіями Co-Co, зменшували інтенсивність флуоресценції. Вимірювання магнітного гістерезису показали, що квантові точки ZnSe, леговані Co, демонструють феромагнетизм при кімнатній температурі, при цьому намагніченість насичення зростає з концентрацією легування до 12%. Феромагнітні властивості були приписані обмінним взаємодіям між іонами Co²⁺ та матрицею ZnSe.

Ключові слова: ZnSe:Co; поверхневий стабілізатор крохмалю; легування кобальтом; магнітні властивості; фотолюмінесценція